12.2 MESOVORTICES FORMED WITHIN BOW ECHOES: THEIR GENESIS AND SENSITIVITY TO THE ENVIRONMENT AND SYSTEM COLD POOL

Nolan T. Atkins and Mike St. Laurent
Lyndon State College, Lyndonville, Vermont

1. INTRODUCTION

Bow echoes are a well-known mode of severe convection capable of producing long swaths of straight-line wind damage and tornadoes (Fujita 1979). The straight-line wind damage swaths may be created by the rear inflow jet (RIJ) descending to the ground near the apex of the bow echo behind the gust front (Fujita 1978). Recent modeling and observational studies (Trapp and Weisman 2003; Atkins et al. 2005; Wakimoto et al. 2006a; Wheatley et al. 2006) have shown that low-level (0-3 km AGL), small-scale (1-10 km) "mesovortices" formed on the bow echo gust front are also capable of producing the straight line wind damage swaths. Damage swaths produced by a mesovortex may not necessarily be located at the bow apex (Atkins et al. 2005). Mesovortices also serve as the parent circulations for tornadoes within bow echoes (e.g., Przybylinski et al. 2000; Atkins et al. 2004; Atkins et al. 2005). It has been shown that the most intense damage produced within a bow echo may be associated with mesovortices (Atkins et al. 2005; Wheatley et al. 2006).

Given their importance in producing surface wind damage, there are still many unanswered questions with respect to the genesis and evolution of mesovortices formed within bow echoes. With respect to their genesis, Trapp and Weisman (2003) have shown that within idealized simulations of bow echoes, mesovortices form in cyclonic/anticyclonic pairs through the tilting of baroclinically-generated horizontal vorticity by convective-scale downdrafts. Convergence of planetary vorticity enhances the cyclonic member of the pair and weakens the anticyclonic circulation. While detailed observations of mesovortex genesis have yet to be collected, published single Doppler studies suggest that cyclonic mesovortices are most often observed within bow echoes. Dual-Doppler data presented by Wakimoto et al. (2007) showed a case where vortex couplets were observed on the bow echo gust front and another with only cyclonic circulations. Thus, the genesis mechanism of bow echo mesovortices is not well understood.

*Corresponding Author Address: Dr. Nolan T. Atkins, Department of Meteorology, Lyndon State College, Lyndonville, VT 05851; email: nolan.atkins@lyndonstate.edu

Single-Doppler observational studies (Atkins et al. 2004, 2005) have also shown that a spectrum of mesovortex strengths are often observed within a bow echo. The stronger, deeper circulations tend to be longer lived and produce surface wind damage. The shallower, weaker circulations are often not damaging. While discriminating between damaging and non-damaging mesovortices has obvious operational detection and warning implications, the dynamical processes that govern vortex strength and longevity are not well understood.

The objectives of this study are therefore to better understand how bow echo mesovortices are forming and what factors control their strength. This will be accomplished by analyzing simulations from the Advanced Research Weather Research and Forecasting (ARW) model (Skamarock et al. 2005) of the 10 June Saint Louis bow echo event that occurred during the Bow Echo and MCV Experiment (BAMEX) (Davis et al. 2004). This particular event produced a total of eleven mesovortices, of which six produced either tornadic or straight-line wind damage. The experimental design is discussed in section 2. A series of sensitivity runs will be shown in section 3 while section 4 presents a discussion of mesovortex genesis. A summary discussion is given in section 5.

2. MODEL FORMULATION AND EXPERIMENTAL DESIGN

All simulations presented herein were performed with the Advanced Research Weather, Research, and Forecast (ARW) model. The horizontal domain size was 225 and 320 km in the west-east and north-south directions, respectively and was sufficiently large such that the convective system did not propagate out of the model domain during the six hour simulation. The domain extended up to 17.5 km in the vertical. The horizontal grid resolution was 750 m for the sensitivity experiments and 500 m for the simulation presented in Section 4 on mesovortex genesis. Vertical grid resolution varied from 160 m near the ground to 600 m at the domain top. As storm motion was subtracted from the sounding winds, the simulated bow echo remained near the center of the model domain. The horizontal boundaries were open. A free-slip boundary condition was specified at the

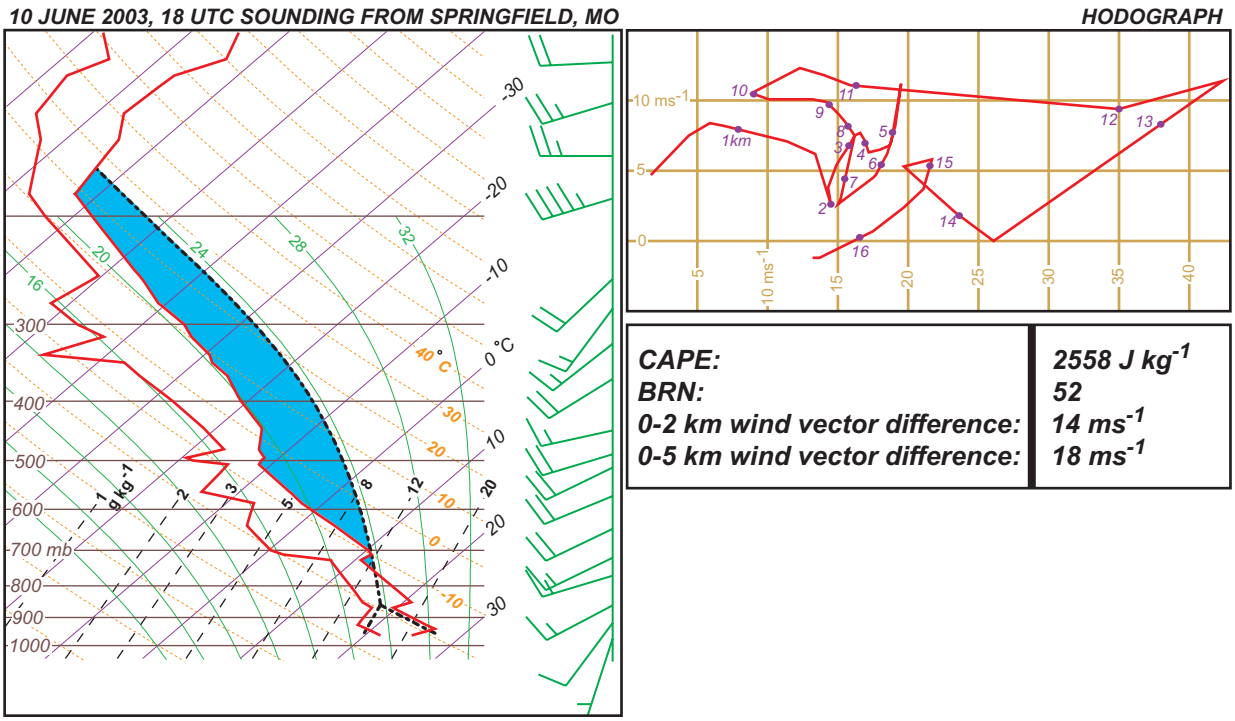

Figure 1. (a) Skew-T diagram of the 18 UTC sounding launched at Springfield, MO on 10 June, 2003. Parcel path is shown as a black-dotted line. Winds are in ms^{-1} (half barb = 2.5 ms^{-1}, full barb = 5 ms^{-1}.) (b) Corresponding hodograph is shown in red.

surface. A Rayleigh damping layer was placed in the upper 5 km of the model domain. Convection was initiated with three warm bubbles 20 km apart in the north-south direction in the center of the model domain. The Coriolis parameter was set to 1x10^{-4} s^{-1} and acted on flow perturbations only. In all experiments, the 1.5 TKE closure scheme available in the ARW model was used to parameterize sub grid-scale turbulence while the Lin et al. (1983) ice scheme was used to parameterize microphysical processes.

The simulations presented herein may be considered to be "quasi-idealized" in that the model domain was initialized with the 10 June 2003 18 UTC Springfield, MO sounding shown in Fig. 1. This sounding was launched in a high equivalent potential temperature air mass that appeared to be representative of the environment that spawned the St. Louis bow echo. The sounding clearly shows an environment containing large convective available potential energy (CAPE) and moderate low-level wind shear.

3. SENSITIVITY EXPERIMENTS

A number of simulations were performed to examine the sensitivity of mesovortex strength and longevity to the system cold pool strength, coriolis forcing, low-level (0-2.5 km) shear, and deeper (0-5 km) shear. These runs were compared to a control run utilizing the Lin ice microphysics scheme, the Coriolis parameter set to 1x10^{-4} s^{-1}, and the wind field was similar to that shown in Fig. 1.

A summary of these sensitivity experiments is shown in Fig. 2 where circulation at the lowest grid level (82 m) is plotted as a function of simulation time. The circulation is computed as $\Gamma = \sum \bar{\zeta} A$ where $\bar{\zeta}$ is the mean vertical vorticity within some area A and the sum is over all mesovortices observed at the lowest grid level. The area *A* is defined as the area of the mesovortex containing vertical vorticity values greater than 1.25x10^{-2} s^{-1} or less than -1.25x10^{-2} s^{-1} for all positive and negative vortices, respectively. This vertical vorticity threshold was subjectively determined and appeared to distinguish well coherent mesovortices from weaker, transient features. Thus, the time series plots in Fig. 2 approximately represent the total circulation produced at the lowest model grid level by mesovortices formed by the convective system.

Results for the cold pool strength experiments are shown in Fig. 2a. The control run where the Lin ice

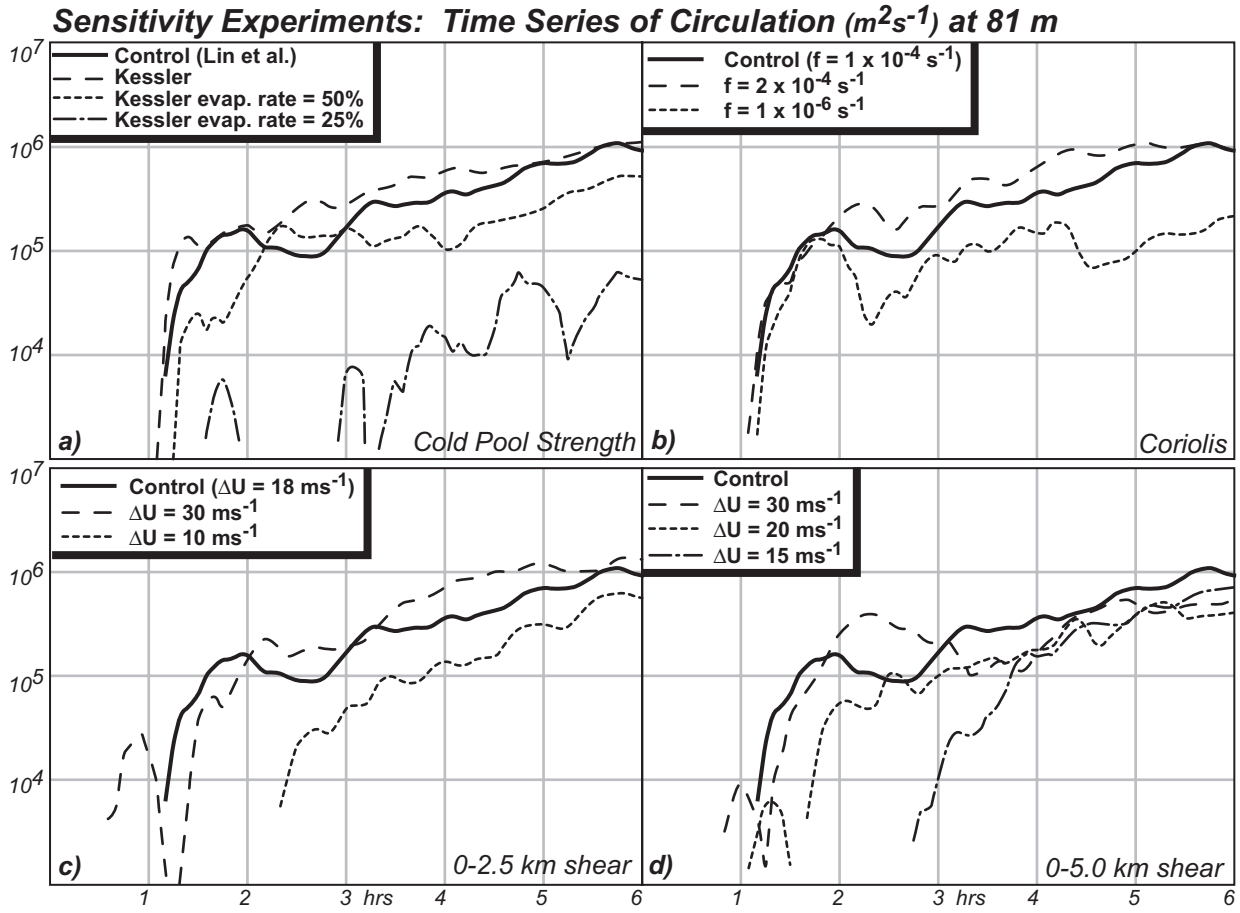

Figure 2. Time series of circulation (m^2s^{-1}) computed at the lowest model grid point (82m) for the (a) cold pool strength, (b) coriolis forcing, (c) low-level shear, and (d) deep shear sensitivity experiments.

microphysics scheme was used, is compared to runs using the Kessler warm rain scheme where the evaporation rate was successively decreased to 50 and 25% of its actual value. The smaller evaporation rates resulted in weaker and smaller cold pools. The results in Fig. 2a clearly show that weaker and small cold pools produce less circulation and therefore fewer and/or weaker mesovortices. Analysis of maximum vertical vorticity at 82 m time series showed that the weaker cold pools produced mesovortices with smaller maximum vertical vorticity values (not shown). The result in Fig. 2a is also partially attributed to the fact that the weaker cold pools are also smaller as they expanded horizontally at a slower rate. This result is shown in Fig. 3 where the fraction of the horizontal domain at 82 m covered by the cold pool is plotted for the same experiments in Fig. 2a. Clearly, as the cold pool strength weakens, its size decreases. Therefore, fewer mesovortices formed simply because there are fewer mesovortex initiation sites on the leading edge of the smaller convective system.

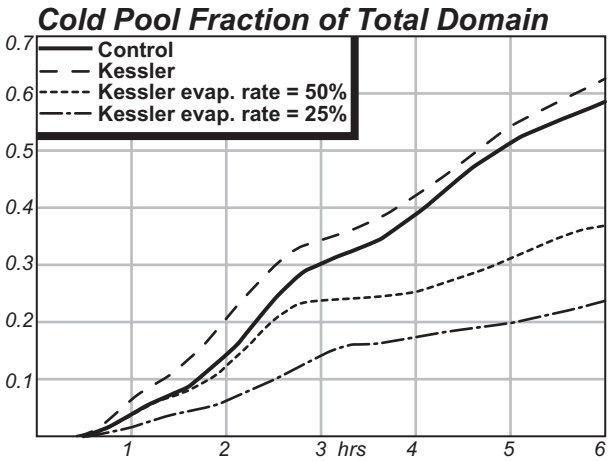

Figure 3. Fraction of horizontal domain at 82m covered by the cold pool for the sensitivity runs shown in Fig. 2a. The cold pool was defined as covering those grid points with a potential temperature perturbation of -1 degree Celsius relative to the base state.

The coriolis forcing sensitivity experiments are shown in Fig. 2b. Relative to the control run, increasing (decreasing) the coriolis parameter leads to more (less) circulation. This result is consistent with those of Trapp and Weisman (2003) who showed that stretching of planetary vorticity is an important contributor to the amplification of cyclonic mesovortices.

Variation of low-level shear is shown in Fig. 2c. Relative to the control run where ΔU is approximately 18 ms^{-1}, increasing the low level shear (ΔU = 30 ms^{-1}) increases the circulation. Decreasing the low-level shear (ΔU = 10 ms^{-1}) decreases the circulation. This behavior can be explained with the cold pool, low-level shear balance discussed by Rotunno et al. (1988). The cold pool intensity *C*, is approximated by:

$$C^2 = 2\int_0^H (-B)dz \qquad (1)$$

where *B* and *H* are the cold pool buoyancy and depth, respectively. When the magnitude of *C* is approximately equal to the wind speed change normal to the convective line orientation and over the depth of the cold pool (ΔU), then the horizontal vorticity produced by the environmental shear and cold pool will balance each other resulting in upright, deep updrafts. When $C/\Delta U < 1$, the updrafts will tilt down shear. Likewise, if $C/\Delta U > 1$, the updrafts will tilt upshear.

Time series of $C/\Delta U$ for the three low-level shear experiments in Fig. 2c are shown in Fig. 3. The cold pool and low-level shear are in approximate balance for the ΔU = 30 ms^{-1} simulation. As the low-level shear decreases, $C/\Delta U$ increases. Thus, the ΔU = 30 ms^{-1} simulation would be associated with stronger, upright updrafts at the leading edge of the convective system. Therefore, vertical vortex stretching would be largest in this simulation. Visual inspection of the stretching tendency term confirms this hypothesis (not shown). Thus, consistent with the circulation time series in Fig. 2c, the strongest mesovortices would be formed when $C/\Delta U$ is approximately equal to 1.

Relative to the control, deeper layer shear appears to have a negative impact on mesovortices as shown in Fig. 2d. All of the deeper layer shear experiments produced circulation that was less than the control. Thus, it appears that while mesovortices may form in deep shear environments, their genesis and subsequent evolution is more sensitive to the magnitude of low-level shear present in the environment.

4. MESOVORTEX GENESIS

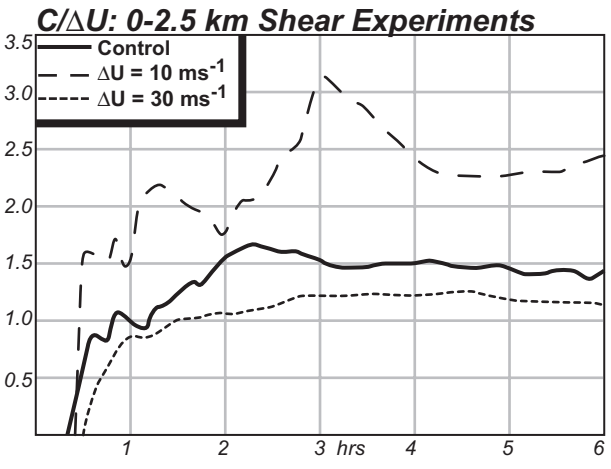

Figure 3. Time series of $C/\Delta U$ for the experiments shown in Fig. 2c. C is a measure of cold pool strength (see text) and ΔU is the wind speed change over the lowest 2.5 km.

To understand how the mesovortices are forming, analysis of a control run with horizontal grid spacing of 500 m is now presented. Shown in Fig. 4 are the gust front and mesovortex positions for the control run during the early and mature stages of the convective system evolution. During the early evolution (Fig. 4a), notice that at least three well-defined cyclonic circulations are observed to intensify in the absence of an anticyclonic circulation. An intensifying anticyclonic vortex is observed at 80 and 85 minutes, however, it does not appear to be associated with a cyclonic circulation. Similar evolution is observed during the mature stage (Fig. 4b) where only cyclonic vortices were observed to initiate and intensify. No cyclonic/anticyclonic vortex pairs were observed during the entire evolution of the convective system. This result suggest that the mesovortex genesis mechanism discussed by Trapp and Weisman (2003) may not be occurring in the control simulation herein.

A detailed analysis of the southern-most mesovortex shown in Fig. 4a at 80 and 85 minutes is presented in Fig. 5. In order to determine where the air creating the mesovortex was originating from, backward parcel trajectories were created and are plotted in Fig. 5a. Notice that an array of trajectories covering much of the vortex are plotted. Two air streams feeding the developing vortex are apparent. The first originates in the inflow. These parcels enter the vortex from low levels and have high values of equivalent potential temperature (θ_e, Fig. 5b). The second source region contains parcels that originate in convective-scale downdrafts north of the developing vortex that travel southward along or behind the gust front. Notice that these parcels contain stream-

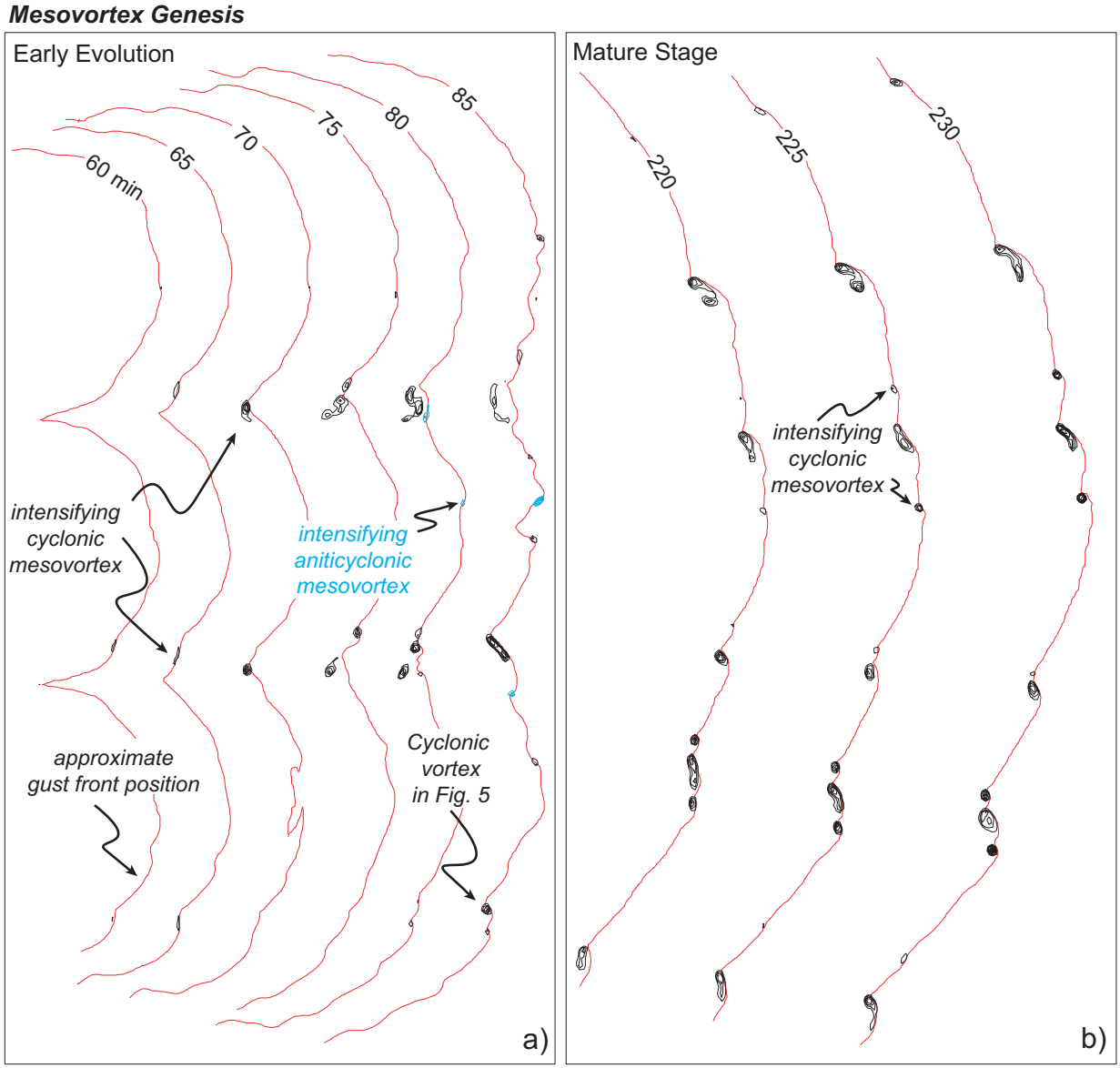

Figure 4. Vertical vorticity and gust front locations during the early and mature stages of the convective system evolution. The gust front locations are shown in red while cyclonic and anticyclonic vertical vorticity is contoured black and light blue, respectively. The first vertical vorticity contour is 1.25x10^{-2} s^{-1}. All data are plotted at 0.2 km.

wise vorticity just prior to reaching the vortex (Fig. 5a). These parcels have much lower θ_e values of approximately 328 K, consistent with the fact that they have descended within convective-scale downdrafts to the north of the vortex. Notice that the mesovortex is located on a gradient of θ_e in Fig. 5b. This observation is consistent with the trajectory analysis in Fig. 5a that shows high θ_e inflow and low θ_e descending parcels populating the resultant mesovortex. The vortex is also embedded within updraft along the gust front (Fig. 5c).

In an effort to determine how these two source regions may be generating a mesovortex, an analysis of the vertical vorticity equation is now given. The equation governing vertical vorticity is, to the inviscid Boussinesq approximation and ignoring frictional effects, given by

$$\frac{\partial \zeta}{\partial t} = -(v \cdot \nabla \zeta) + \omega_H \cdot \nabla_H w + \zeta \frac{\partial w}{\partial z} \qquad (2)$$

where the subscript *H* denotes the horizontal component of a vector. The terms on the rhs of (2) physically represent the advection, tilting and stretching of vertical vorticity, respectively.

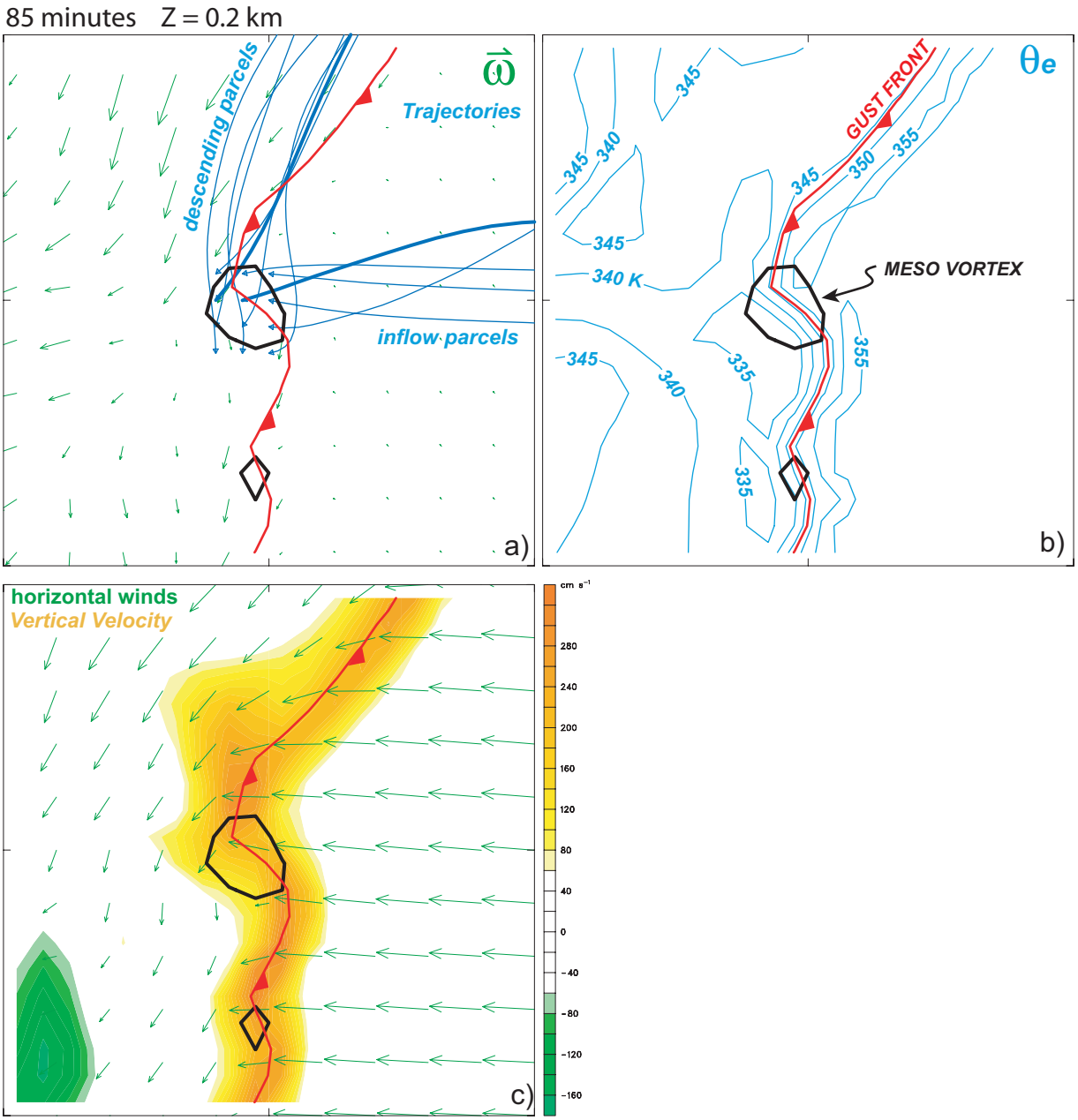

Figure 5. Analysis of the southern-most vortex at 80 and 85 minutes shown in Fig. 4. In all panels, the black contour indicating the vortex position corresponds to the 1.25 x 10^{-2} s^{-1} vertical vorticity contour. The red line is the approximate gust front position. (a) Horizontal vorticity vectors (green) and backward parcel trajectories (blue) released at the arrowhead locations at 0.2 km. The thick parcel paths correspond to those shown in Fig. 6. (b) Equivalent potential temperature (K) is plotted in blue. (c) Vertical velocity is shown with the color scale to the right of the panel.

Time series of vertical vorticity and integrated stretching and tilting tendency terms along parcel paths originating in the inflow and descending from the north are plotted in Fig. 6. The time series data in Fig. 6 represent 20 minutes of data prior to the release time at 85 minutes. In Fig. 6a, the descent of the parcel at the earlier times is evident. Just as the parcel reaches low levels (< 100 m) at 76 minutes, it encounters positive tilting that in turn creates weak positive vertical vorticity. Recall that the descending parcels appear to have positive

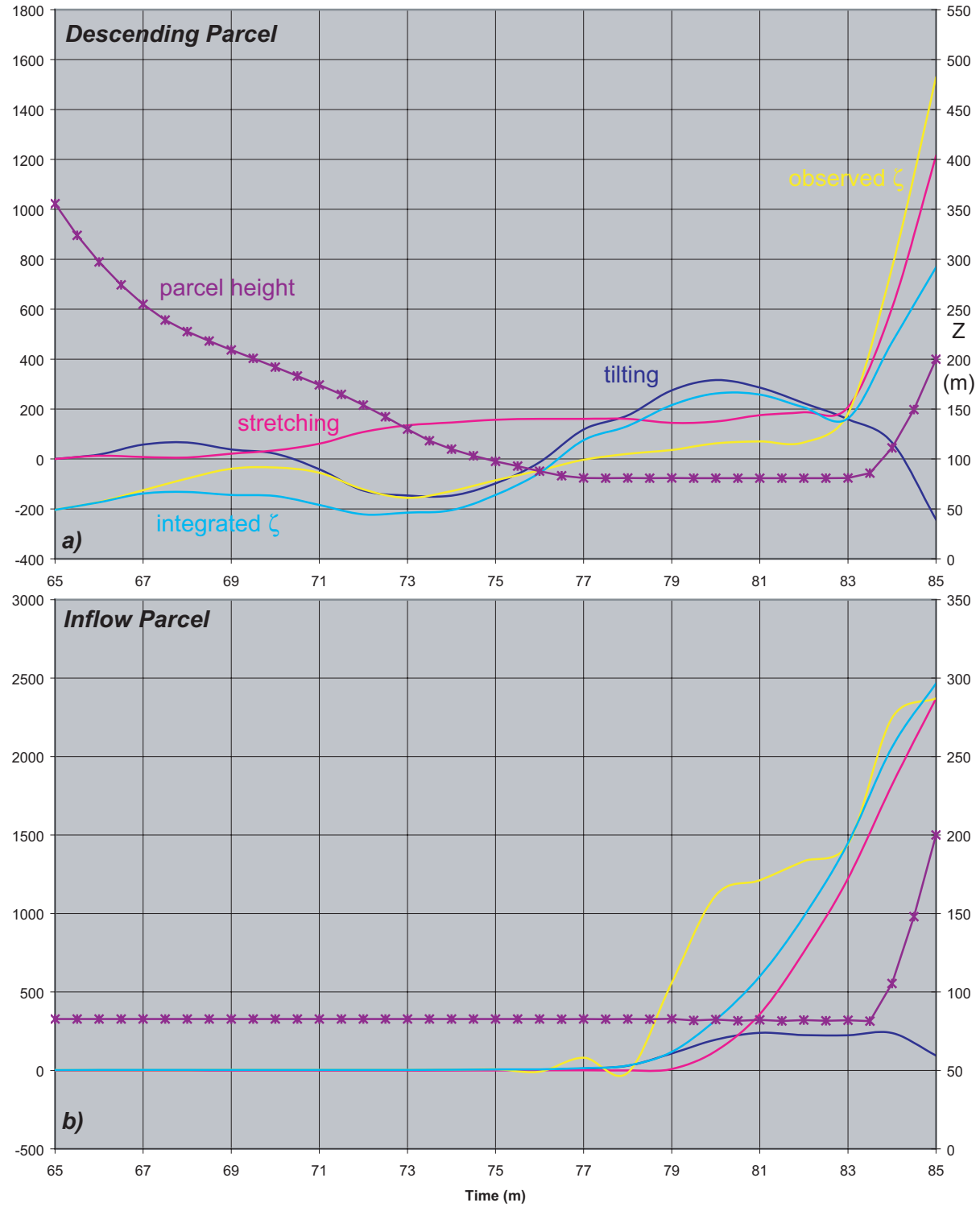

Figure 6. Time series of observed (yellow) and integrated (light blue) vertical vorticity (x 10^{-5} s^{-1}) for a descending (a) and inflow (b) parcel. The parcel trajectories are shown as thick blue lines in Fig. 5a. Integrated tilting (dark blue) and stretching (red) tendency terms are plotted along with parcel height (purple).

streamwise vorticity as they approach the vortex (Fig. 5a). As the parcel continues to approach the vortex, it then encounters strong stretching at 83 minutes which then quickly amplifies the vertical vorticity of the parcel.

The inflow parcel data along the trajectory path in Fig. 5a is shown in Fig. 6b. The parcel height remains at the lowest grid level until it reaches the gust front where it ascends to the final altitude of 200 m. Notice that the parcel encounters positive tilting beginning at about 78 minutes creating positive vertical vorticity. This is due to the parcel having a small amount of positive streamwise vorticity generated by the environmental shear that is then tilted by the updraft associated with the gust front. The tilted streamwise vorticity is then strongly amplified by through stretching. For both parcels, the integrated vorticity produced by tilting and stretching is in close agreement with the observed parcel vertical vorticity.

The above analysis is consistent with the explanation of low-level mesocyclogenesis within supercells put forth by Rotunno and Klemp (1985). Their analysis clearly showed two source regions of air feeding the low-level mesocyclone. One originated within the inflow and the other descended from aloft and was associated with lower values of θ_e. From a vorticity analysis point of view, it was argued that parcels traveled along the storms forward flank downdraft acquiring horizontal streamwise vorticity that was then tilted and stretched by the updraft. This scenario is similar to what has been presented in Section 4 herein for mesovortices formed in the early stages of the convective system evolution.

5. Summary

Preliminary results on the genesis of mesovortices formed within bow echoes and factors that control their strength have been presented for a quasi-idealized simulations of the 10 June 2003 bow echo event observed during BAMEX. Through analysis of low-level circulation produced by mesovortices, a series of sensitivity experiments have shown that stronger cold pools, larger Coriolis forcing, sufficient low level shear such that $C/\Delta U$ is approximately one all contribute to stronger, longer lived mesovortices. Physically, stretching of planetary vorticity enhances cyclonic mesovortices as shown by Trapp and Weisman (2003). When the cold pool strength and low-level shear are in approximate balance ($C/\Delta U = 1$), the strongest mesovortices are observed. This may be explained by the fact that the stretching tendency term in (2) will be largest and deepest since the updrafts will be upright and most intense. Recall that for the vortex shown in Fig. 5, the stretching tendency term was shown to quickly amplify the vertical vorticity associated with the mesovortex.

During the early evolution of the convective system, two air source regions were identified feeding the resultant mesovortex. The first originated aloft within convective-scale downdrafts having low θ_e values. The second originated within the environmental inflow. Consistent with these two source regions, the mesovortex formed on a gradient of θ_e. The mesovortex appeared to form by the tilting and stretching of parcels that have acquired horizontal streamwise vorticity primarily behind the gust front and to a lesser extent from the environmental inflow. Note that this mechanism will produce only cyclonic mesovortices. Indeed, no cyclonic/anticyclonic mesovortex pairs were observed at any point during the control run simulation.

Future work will focus on understanding the genesis of the mesovortices from a circulation perspective. Mesovortices formed during the mature stage will also be studied. Finally, an investigation of primarily single-Doppler radar data capturing the genesis of mesovortices formed within bow echoes will be studied to determine whether cyclonic only or cyclonic/anticyclonic pairs are observed. Such information will aid our interpretation of the modeling results presented herein.

Acknowledgements: The research results presented herein were supported by the National Science Foundation under Grant ATM-0630445 and Vermont EPSCoR EPS-0236976.

References

Atkins, N.T., J.M. Arnott, R.W. Przybylinski, R.A. Wolf, and B.D. Ketcham, 2004: Vortex structure and evolution within bow echoes. Part I: Single-Doppler and damage analysis of the 29 June 1998 Derecho. *Mon. Wea. Rev.*, **132**, 2224-2242.

_____, C.S. Bouchard, R.W. Przybylinski, R.J.Trapp, and G. Schmocker, 2005: Damaging surface wind mechanism within the 10 June 2003 Saint Louis bow echo during BAMEX. *Mon. Wea. Rev.*, **133**, 2275-2296.

Fujita, T.T., 1978: Manual of downburst identification for project Nimrod. Satellite and Mesometeorology Research Paper 156, Dept. of Geophysical Sciences, University of Chicago, 104 pp. [NTIS PB-286048]

_____, 1979: Objectives, operation, and results of project NIMROD. Preprints, *11th Conf. on Severe Local Storms*, Kansas City, MO, Amer. Meteor. Soc., 259-266.

Przybylinski, R.W., G.K. Schmocker, and Y-J. Lin, 2000: A study of storm and vortex morphology during the 'intensifying stage' of severe wind mesoscale convective systems. Preprints, *20th Conf. on Severe Local Storms,* Orlando, FL, Amer. Meteor. Soc., 173-176.

Rotunno, R., and J. B. Klemp, 1985: On the rotation and propagation of simulated supercell thunderstorms. *J. Atmos. Sci.*, **42,** 271- 292.

Skamarock, W. C., J. B. Klemp, J. Dudia, D. O. Gill, D. M. Barker, W. Wang, and J. G. Powers, 2005: A description of the Advanced Research WRF version 2. NCAR Tech. Note NCAR/TN-468+STR, 100 pp.

Trapp, R.J. and M.L. Weisman, 2003: Low-level mesovortices within squall lines and bow echoes. Part II: Their genesis and implications. *Mon. Wea. Rev.*, **131**, 2804-2823.

Wakimoto, R.M., H.V. Murphy, A. Nester, D.P. Jorgensen, and N.T. Atkins, 2006: High winds
generated by bow echoes. Part I: Overview of the Omaha bow echo 5 July 2003 storm during BAMEX. *Mon. Wea. Rev.,* **134**, 2793-2812

Wheatley, D.M., R.J. Trapp, and N.T. Atkins, 2006: Radar and damage analysis of severe bow echoes observed during BAMEX. *Mon. Wea. Rev.*, **134**, 791-806.